2017 IEEE 67th Electronic Components and Technology Conference

Finite Elements for Electromigration Analysis

Elena E. Antonova and David C. Looman
ANSYS, Inc.
2600 Ansys Drive, Canonsburg, PA 15317, USA
elena.antonova@ansys.com
dave.looman@ansys.com

***Abstract*—A finite element analysis of the electromigration process in metal interconnects can now be performed using the ANSYS program. The analysis is based on the model that includes all the driving forces of electromigration—diffusion gradient, electric current, stress, and temperature gradients. The electromigration model is implemented in the framework of 2-D and 3-D coupled-field elements. Diffusion, electric, structural, and thermal degrees of freedom are fully (matrix) coupled and solved for simultaneously. Matrix coupling ensures robust convergence of the highly nonlinear electromigration analysis. The finite element solution is validated using 1-D analytical and numerical models of the electromigration process in metal lines. A model of a solder joint illustrates a 3-D electromigration analysis.**

Keywords- finite elements; electromigration; diffusion; stress migration; thermomigration; reliability

I. INTRODUCTION

Electromigration is the process of mass transport in metal interconnects induced by high density electric currents. Two types of electric forces initiate atomic migration in metals: (1) electrostatic force acting on the atom in the direction of the electric field and (2) collision force, or momentum exchange, between the atoms and the electrons drifting in the direction opposite to the electric field. Although these forces are the cause of electromigration, they alone do not drive the atomic transport. Intense electric currents in interconnects are accompanied by the gradients of atomic concentration, mechanical stress, and temperature. These gradients become the driving forces of mass transport along with the electric current. Gradual displacement of metal atoms from their positions in the lattice can result in macroscopic mass depletion or mass accumulation. Over time, voids or hillocks can form, eventually leading to interconnect failure in the form of an open or short circuit.

Electromigration is a leading failure mechanism in integrated circuits (ICs) where current densities are high due to miniaturization and use of thin film conductors. As such, it has been a focus of intense experimental study and numerical simulation. Accurate numerical models of electromigration can complement laboratory testing by predicting the reliability of IC interconnects in terms of their time-to-failure (TTF). Such models should address the complex interactions between diffusion, electric, thermal, and mechanical forces and fields taking place in the interconnects. Ideally, other factors affecting the electromigration process should also be taken into consideration. These include void nucleation and growth in metal lines, formation of intermetallic compounds (IMC) in solder bumps, and the effect of the metal's microstructure. To calculate the TTF, failure criteria related to either void concentration, hydrostatic stress, or divergence of diffusion flux also need to be established.

One-dimensional (1-D) analytical and numerical models of vacancy and stress evolution have been used to predict the TTF of confined aluminum lines [1-3]. However, simulating the damage caused by electromigration in more complex interconnects would require a three-dimensional (3-D) numerical model. The finite-element (FE) method is a natural choice for such advanced models as it can easily handle arbitrary 3-D geometries, multiple physics, and various loads and boundary conditions, and it can be adapted to coupled-field and highly nonlinear constitutive models. The FE method has already been applied to the simulation of electromigration in solder joints [4], through-silicon vias (TSVs) [5], copper dual-damascene structures [6], and standard wafer electromigration accelerated test (SWEAT) structures [7]. In most cases, a commercial finite element package has been adapted or customized to handle a version of the electromigration model.

The ANSYS finite element program has been routinely used to simulate electronic packaging; for example, to predict mechanical reliability of solder joints, thermal cycling reliability of flip chip interconnects, and moisture related reliability of mold compounds. In response to the increased demand for electromigration reliability simulation, ANSYS coupled-physics capabilities have been extended to support an electromigration analysis in metal interconnects. This paper proposes a general finite element model of the electromigration process driven by diffusion, electric current, stress gradient, and temperature gradient. Implementation details are presented and illustrated with several numerical examples.

II. GOVERNING EQUATIONS

It is generally accepted that atomic migration in metal interconnects is driven by the electric current (electrostatic force and electron wind) and by the gradients of atomic concentration (diffusion proper), hydrostatic stress (stress-migration), and temperature (thermo-migration). To include these driving forces in the electromigration model, the first Fick's law of diffusion describing atomic flux $\mathbf{J}_a$ is written in the form:

2377-5726/17 $31.00 © 2017 IEEE
DOI 10.1109/ECTC.2017.310

$$\mathbf{J}_a = -\frac{[D]}{kT} C \nabla \mu, \tag{1}$$

where $[D]$ is the atomic diffusivity matrix, k is Boltzmann's constant, T is the absolute temperature, and μ is the generalized chemical potential derived from atomic concentration C, electric potential φ, hydrostatic stress σ_H, and temperature T as shown in Table I.

TABLE I. DRIVING FORCES OF ELECTROMIGRATION

Process	Chemical Potential μ	Force $F=-\nabla\mu$	Flux $J=(D/kT)cF$
Diffusion	$kT\ln C$	$-kT\nabla C/C$	$-D\nabla C$
Electro-migration	$Z^*e\varphi$	$-Z^*e\nabla\varphi$	$-(D/kT)CZ^*e\nabla\varphi$
Stress-migration	$-\Omega\sigma_H$	$\Omega\nabla\sigma_H$	$(D/kT)C\Omega\nabla\sigma_H$
Thermo-migration	$(Q/T)T$	$-(Q/T)\nabla T$	$-(D/kT^2)CQ\nabla T$

Substituting the driving forces from Table I in (1), the total atomic flux of electromigration can be written as:

$$\mathbf{J}_a = -[D]\nabla C - \frac{[D]CZ^*e}{kT}\nabla\varphi + \frac{[D]C\Omega}{kT}\nabla\sigma_H - \frac{[D]CQ}{kT^2}\nabla T, \tag{2}$$

where Z^* is the effective charge number of the atom that combines the effects of the electrostatic and the electron wind forces, e is the elementary charge, Ω is the atomic volume, and Q is the heat of atomic transport. The hydrostatic stress is defined as the average of principal stresses $\sigma_H = (\sigma_{11} + \sigma_{22} + \sigma_{33})/3 = \mathrm{tr}(\sigma_{ii})/3$, where tr denotes the trace operator.

The constitutive relation for the atomic flux (2) couples the atomic concentration with the electric potential, mechanical stress, and temperature. Therefore, in an electromigration analysis the *mass balance* equation, or second Fick's law, that controls the change of atomic concentration over time:

$$\frac{\partial C}{\partial t} + \nabla\cdot\mathbf{J}_a = \dot{g}, \tag{3}$$

where $\dot{g}$ is the atom generation rate per unit volume, must be solved together with the *electric charge conservation* equation, the *heat transfer* equation, and *Newton's second law* as shown below.

Electric Charge Conservation:

$$\nabla\cdot\mathbf{j} = 0, \tag{4}$$

where $\mathbf{j}$ is the electric current density.

Heat Transfer:

$$\rho c\frac{\partial T}{\partial t} + \nabla\cdot\mathbf{q} = \dot{q}, \tag{5}$$

where ρ is the mass density, c is specific heat, $\mathbf{q}$ is the heat flux vector, and $\dot{q}$ is the heat generation rate per unit volume.

Newton's second law:

$$\rho\frac{\partial^2\mathbf{u}}{\partial t^2} + \varsigma\frac{\partial\mathbf{u}}{\partial t} + \nabla\cdot\boldsymbol{\sigma} = \mathbf{f}, \tag{6}$$

where $\mathbf{u}$ is the displacement vector, ς is the damping coefficient, and $\mathbf{f}$ is the force load vector.

Note that (4) was written without the displacement current term as the latter is insignificant in metals. Also, for electromigration applications, the dynamic terms in (6) can be ignored.

To complete the system of governing equations, constitutive relations for the electric current density $\mathbf{j}$, mechanical stress $\boldsymbol{\sigma}$, and thermal flux $\mathbf{q}$ should be considered along with (1). These constitutive relations can include multiple coupled-field effects [8], but only those relevant to the process of electromigration are considered here:

$$\mathbf{j} = [\sigma]\mathbf{E}, \tag{7}$$

where $[\sigma]$ is the electric conductivity matrix and $\mathbf{E} = -\nabla\varphi$ is the electric field;

$$\boldsymbol{\sigma} = [c]\boldsymbol{\varepsilon}^{el}, \tag{8}$$

where $[c]$ is the elasticity matrix and $\boldsymbol{\varepsilon}^{el}$ is the elastic strain vector; and

$$\mathbf{q} = [k]\nabla T, \tag{9}$$

where $[k]$ is the thermal conductivity matrix.

Equations (7) and (9) imply that atomic diffusion does not contribute to the electric current density $\mathbf{j}$ or thermal flux $\mathbf{q}$. In other words, the electric current of migrating atoms and the heat of diffusion (Dufour effect) are ignored in the electromigration model.

The elastic strain in (3) can be derived from the total strain $\boldsymbol{\varepsilon} = \nabla\mathbf{u}$ by subtracting all the non-elastic types of stain:

$$\boldsymbol{\varepsilon}^{el} = \boldsymbol{\varepsilon} - \boldsymbol{\varepsilon}^{pl} - \boldsymbol{\varepsilon}^{th} - \boldsymbol{\varepsilon}^{di} - \ldots, \tag{10}$$

where $\boldsymbol{\varepsilon}^{pl}$, $\boldsymbol{\varepsilon}^{th}$, $\boldsymbol{\varepsilon}^{di}$ are the plastic, thermal expansion, and diffusion expansion strains, respectively. By analogy with thermal strain,

$$\boldsymbol{\varepsilon}^{th} = \{\alpha\}\left(T - T_{ref}\right) = \{\alpha\}\Delta T\,, \tag{11}$$

where $\{\alpha\}$ is the vector of coefficients of thermal expansion and T_{ref} is the reference temperature for the thermal strain calculation, the diffusion strain is defined as follows:

$$\boldsymbol{\varepsilon}^{di} = \{\beta\}\left(C - C_{ref}\right) = \{\beta\}\Delta C\,, \tag{12}$$

where $\{\beta\}$ is the vector of coefficients of diffusion expansion and C_{ref} is the reference concentration for the diffusion strain calculation. Retaining only those strains in (10) needed for coupling with the atomic flux, we obtain the following equation for stress:

$$\boldsymbol{\sigma} = [c]\left(\nabla\mathbf{u} - \{\alpha\}\Delta T - \{\beta\}\Delta C\right). \tag{13}$$

Substituting (13) into (2) reveals a complex dependence of atomic flux on concentration, electric potential, temperature, and mechanical deformation:

$$\begin{aligned}\mathbf{J}_a = &-\left([D] + \frac{[D]C\Omega}{3kT}\,\mathrm{tr}([c]\{\beta\})\right)\nabla C \\ &- \frac{[D]CZ^*e}{kT}\nabla\varphi \\ &+ \frac{[D]C\Omega}{3kT}\,\mathrm{tr}([c])\nabla(\nabla\mathbf{u}) \\ &- \left(\frac{[D]CQ}{kT^2} + \frac{[D]C\Omega}{3kT}\,\mathrm{tr}([c]\{\alpha\})\right)\nabla T\end{aligned}\,. \tag{14}$$

Equation (14) shows that diffusion expansion contributes to the diffusion driving force (*backflow*), and the thermal expansion contributes to the thermomigration driving force.

In addition to constitutive relations, the equations governing the process of electromigration are coupled by Joule heat generation:

$$\dot{q}_J = \mathbf{j}\cdot\mathbf{E} \tag{15}$$

and through the temperature dependence of the material properties.

III. Finite Element Formulation

Following the finite element discretization of the problem domain, the unknown concentration C, electric potential φ, components u_{i} of the mechanical displacement vector $\mathbf{u} = \{u_1, u_2, u_3\}^{\text{T}}$, and temperature T are approximated over the finite element as:

$$C = \mathbf{N}\cdot C_e\,, \tag{16}$$

$$\varphi = \mathbf{N}\cdot\varphi_e\,, \tag{17}$$

$$u_i = \mathbf{N}\cdot u_{ie}, \tag{18}$$

$$T = \mathbf{N}\cdot T_e\,, \tag{19}$$

where $\mathbf{N}$ is the vector of element shape functions, C_{e} is the vector of nodal concentrations, φ_{e} is the vector of nodal electric potentials, T_{e} is the vector of nodal temperatures, and $\mathbf{u}_{\text{e}}$ is the vector of nodal mechanical displacements. The system of finite element equations can be obtained by applying the Galerkin method of weighted residuals to the governing equations of electromigration discussed in the previous section:

$$\begin{bmatrix} C_{CC} & 0 & 0 & 0 \\ 0 & 0 & 0 & 0 \\ 0 & 0 & 0 & 0 \\ 0 & 0 & 0 & C_{TT} \end{bmatrix}\begin{Bmatrix} \dot{C}_e \\ \dot{\varphi}_e \\ \dot{\mathbf{u}}_e \\ \dot{T}_e \end{Bmatrix} + \begin{bmatrix} K_{CC} & K_{C\varphi} & K_{Cu} & K_{CT} \\ 0 & K_{\varphi\varphi} & 0 & 0 \\ K_{uC} & 0 & K_{uu} & K_{uT} \\ 0 & 0 & 0 & K_{TT} \end{bmatrix}\begin{Bmatrix} C_e \\ \varphi_e \\ \mathbf{u}_e \\ T_e \end{Bmatrix} = \begin{Bmatrix} G \\ I \\ \mathbf{F} \\ Q + Q_J \end{Bmatrix}, \tag{20}$$

where the element matrices and load vectors are calculated by numerical integration over the element volume V as follows:

$C_{CC} = \int_V \mathbf{N}\mathbf{N}dV$ - diffusion damping matrix,

$C_{TT} = \rho c\int_V \mathbf{N}\mathbf{N}dV$ - specific heat matrix,

$K_{CC} = \int_V \frac{\partial(\nabla\cdot\mathbf{J}_a)}{\partial C}dV$ - diffusivity matrix

$K_{\varphi\varphi} = \int_V \nabla\mathbf{N}\cdot[\sigma]\cdot\nabla\mathbf{N}dV$ - electric conductivity matrix,

$K_{uu} = \int_V \mathbf{B}\cdot[c]\cdot\mathbf{B}dV$ - elastic stiffness matrix, and $\mathbf{B}$ is the strain –displacement matrix,

$K_{TT} = \int_V \nabla\mathbf{N}\cdot[k]\cdot\nabla\mathbf{N}dV$ - thermal conductivity matrix,

$K_{uT} = -\int_V \mathbf{B}\cdot[c]\cdot\{\alpha\}\cdot\mathbf{N}dV$ - thermal strain matrix,

$K_{uC} = -\int_V \mathbf{B}\cdot[c]\cdot\{\beta\}\cdot\mathbf{N}dV$ - diffusion strain matrix,

$K_{C\varphi} = \int_V \frac{\partial(\nabla\cdot\mathbf{J}_a)}{\partial\varphi}dV$ - electric migration matrix,

$K_{Cu} = \int_V \frac{\partial(\nabla\cdot\mathbf{J}_a)}{\partial\mathbf{u}}dV$ - mechanical migration matrix,

$K_{CT} = \int_V \frac{\partial(\nabla\cdot\mathbf{J}_a)}{\partial T}dV$ - thermal migration matrix,

$Q_J = \int_V \mathbf{N}\mathbf{J} \cdot \mathbf{E} dV$ - Joule heat load vector.

Terms G, I, Q, $\mathbf{F}$ are the atom generation rate, electric current, heat generation rate, and the mechanical force load vectors, respectively.

The matrices K_{CC}, $K_{C\varphi}$, K_{Cu}, and K_{CT} above are given in a symbolic form as their derivation is too involved. Full expressions for these matrices are obtained by differentiating the atomic flux (14) divergence $\nabla \cdot \mathbf{J}_a$ with respect to the concentration C, electric potential φ, mechanical displacement u, and temperature T. The derivation of matrices is detailed here for the simple case when the atomic transport is driven by the electric field alone. In this case (14) reduces to:

$$\mathbf{J}_a = -[D]\nabla C - \frac{[D]CZ^*e}{kT}\nabla\varphi, \tag{21}$$

and matrices $K_{C\varphi}$ and K_{CC} are expressed using the element shape functions as:

$$\begin{aligned} K_{C\varphi} &= \int_V \frac{\partial(\nabla \cdot \mathbf{J}_a)}{\partial\varphi} dV \\ &= \int_V \nabla\mathbf{N} \cdot \frac{C[D]Z^*e}{kT} \cdot \nabla\mathbf{N} dV \end{aligned}, \tag{22}$$

$$\begin{aligned} K_{CC} &= \int_V \frac{\partial(\nabla \cdot \mathbf{J}_a)}{\partial C} dV \\ &= \int_V \nabla\mathbf{N} \cdot [D] \cdot \nabla\mathbf{N} dV \\ &\quad - \int_V \nabla\mathbf{N} \cdot \frac{[D]Z^*e}{kT} \cdot \mathbf{E} \cdot \mathbf{N} dV \end{aligned}. \tag{23}$$

Therefore, in the finite element formulation, the electric driving force is represented by matrix $K_{C\varphi}$ (22) that couples the element nodal concentrations C_e and electric potentials φ_e, and by the electric field ($\mathbf{E}$) dependent term of the diffusion matrix K_{CC} (23). Matrices K_{Cu} and K_{CT} are derived analogously to $K_{C\varphi}$ in (22). Matrix K_{CC} gets more terms similar to the second part of (23) as a result of the differentiation of $\nabla \cdot \mathbf{J}_a$ with respect to C.

The finite element system (20) is nonsymmetric and nonlinear. Its solution yields concentrations C_e, electric potentials φ_e, displacements $\mathbf{u}_e$, and temperatures T_e at the unconstrained element nodes. The nodal solution can be post-processed to calculate the gradient of concentration ∇C, electric field $\mathbf{E}$, total strain $\boldsymbol{\varepsilon}$, and the gradient of temperature as follows:

$$\nabla C = \nabla\mathbf{N} \cdot C_e, \tag{24}$$

$$\mathbf{E} = -\nabla\mathbf{N} \cdot \varphi_e, \tag{25}$$

$$\boldsymbol{\varepsilon} = \mathbf{B} \cdot \mathbf{u}, \tag{26}$$

$$\nabla T = \nabla\mathbf{N} \cdot T_e. \tag{27}$$

The values of atomic flux $\mathbf{J}_a$ (14), electric current density $\mathbf{j}$ (7), mechanical stress $\boldsymbol{\sigma}$ (13), and heat flux $\mathbf{q}$ (9) can then be calculated using (24)-(27).

IV. Finite Element Implementation

Electromigration analysis is available with the ANSYS family of coupled-field elements: PLANE223 (8-node quadrilateral), SOLID226 (20-node hexahedron), and SOLID227 (10-node tetrahedron) [9]. These elements were designed to solve 2-D and 3-D multiphysics problems in one single solution; that is, by using a single mesh of coupled-field elements, applying the relevant material properties and boundary conditions to one model, solving for all the degrees of freedom (DOFs) simultaneously, and post-processing one set of results.

Each element supports multiple DOFs per node, including concentration, electric potential, mechanical displacements, and temperature needed to model the process of electromigration. These DOFs can be turned on and off depending on the combination of physics needed for the analysis. For example, to calculate the evolution of atomic concentration as a function of electric current only, it is sufficient to select a diffusion-electric combination of DOFs. If stress evolution is of interest, a diffusion-electric-structural analysis option can be used. Thermal effects can be activated by adding the temperature DOF to the analysis. It should be noted, however, that the more DOFs per node that are active, the larger the model and the higher the memory and computational time requirements. The combination of diffusion, electric, structural, and thermal degrees of freedom is also supported by 2-D (CONTA171, CONTA172) and 3-D (CONTA173, CONTA174) contact elements that can be used to connect dissimilar meshes or model imperfect contact.

The electromigration analysis is inherently nonlinear due to the dependency of its driving forces and material properties on temperature and concentration. Other material and geometric nonlinearities may be incorporated in the analysis. Therefore, the analysis requires an iterative solution using the Newton-Raphson method. Nonlinear solution convergence is robust due to the matrix coupling between the element DOFs in (20). A nonlinear solution also implies that the electromigration analysis can be steady-state or time-transient.

Material definition for the migration model includes the input of parameters controlling the atomic flux (2) and the input of material properties associated with the constitutive relations (7), (8), (9), (11) and (12). The effective charge number, atomic volume, and heat of transport are scaled with respect to the Boltzmann constant k and input as Z^*e/k, Ω/k, and Q/k using a special migration model [10]. The

same model is also used to input the activation energy E_a/k for the temperature dependent diffusivity coefficient $D = D_0 \exp(-E_a / kT)$. To accommodate the applications where concentration is measured in moles, the same parameters can be input as Z^*F/R, Ω/R, Q/R, and E_a/R, where R is the universal gas constant, F is the Faraday constant, and Ω and Q are the molar volume and molar heat of transport, respectively. The matrices of diffusivity [D], electrical resistivity [ρ]= [σ]$^{-1}$, elasticity [c], and thermal conductivity [k], as well as the vectors of thermal ({α}) and diffusion ({β}) expansion coefficients are defined as orthotropic material properties by their components in the x, y, z directions. Mass density ρ, specific heat c, as well as reference temperature T_{ref} and concentration C_{ref}, are input as scalar material properties.

The migration model distinguishes between atomic and vacancy fluxes. The differences between the two constitutive models are summarized in Tables II and III.

TABLE II. ATOMIC MIGRATION MODEL

Flux	$\mathbf{J}_a = -[D]\nabla C + \frac{[D]Cz^*e}{kT}\mathbf{E} + \frac{[D]C\Omega}{kT}\nabla\sigma_H - \frac{[D]CQ}{kT^2}\nabla T$
Electric field	**J***a* opposite to **E** ($Z^* < 0$)
Stress gradient	**J***a* along $\nabla\sigma_H$
Volume Change $\varepsilon^{di} = \{\beta\}\Delta C$	Expansion ($\beta > 0$)

TABLE III. VACANCY MIGRATION MODEL

Flux	$\mathbf{J}_v = -[D]\nabla C + \frac{[D]Cz^*e}{kT}\mathbf{E} - \frac{[D]Cf\Omega}{kT}\nabla\sigma_H - \frac{[D]CQ}{kT^2}\nabla T$
Electric field	**J***v* along **E** ($Z^* > 0$)
Stress gradient	**J***v* opposite to $\nabla\sigma_H$
Volume change $\varepsilon^{di} = \{\beta\}\Delta C$	Contraction ($\beta < 0$)

The fact that the atoms migrate in the direction of the electron wind, that is, opposite to the electric field **E**, while the vacancies migrate in the direction of the electric field is reflected in the sign of the effective charge number Z^*, which is negative for atomic electromigration and positive for vacancy electromigration. Also, vacancies migrate in the direction opposite to the gradient of hydrostatic stress because the effective volume of a vacancy $f\Omega$ ($0 < f < 1$) is smaller than the volume of the atom it replaces [11], thus causing relaxation of the neighboring atoms and contraction of the volume $\boldsymbol{\varepsilon}^{di} = \{\beta\}\Delta C$ ($\beta < 0$). While the signs of the driving forces are embedded in the FE formulation, it is the user's responsibility to assign a correct sign to the charge number Z^* and to the expansion coefficient β.

Since the electromigration analysis was developed based upon the existing structural-thermal, structural-diffusion, and thermo-electric capabilities of the coupled-field elements, it inherited the material models, loads, and coupled-field effects applicable to a given combination of DOFs. For example, structural rate-dependent plasticity models (e.g., Anand viscoplasticity) can be used together with the electromigration model to perform a reliability analysis of a solder joint. All types of diffusion, electric, structural, and thermal loads available with the ANSYS program are also available with the electromigration analysis. Coupled-field capabilities such as piezoresistivity or thermoplastic effect can be superimposed on electromigration.

In the present FE electromigration analysis, material properties and loads can be functions of time (t), position (x, y, z), temperature (T), concentration (C), and hydrostatic stress (σ_H). This feature currently applies to the coefficients of diffusivity [D], electrical resistivity [ρ], and diffusion expansion {β}. Reference (equilibrium) concentration C_{ref}, and diffusion loads (surface flux and generation rate) can also be functions of these state variables. This capability can be used to customize the constitutive relations or loads, to define failure criteria, or to specify a non-uniform material distribution. As examples, consider the following potential applications:

- The dependence of electrical resistivity on concentration [$\rho(C)$] can be used to simulate electric failure due to void formation.
- Spatially dependent diffusivity [$D(x,y,z)$] can be used to define electromigration paths along the metal grain boundaries.
- A concentration dependent generation rate $G(C)$ can be used to define the source term $G = -(C - C_e)/\tau_s$ [2] that describes the annihilation or generation of vacancies.

Some of these dependencies were used in the examples presented in the following sections.

V. TRANSIENT ANALYSIS OF A METAL LINE

The electromigration analysis was first applied to 1-D models of thin and narrow aluminum interconnect lines considered in [1-3]. This simple configuration served to validate the analysis and to illustrate some important aspects of our electromigration model. Unless otherwise stated, the following parameters for the aluminum line from [3] were used in the numerical examples:

- Line length L = 50 μm,
- Current density J_e = 1MA/cm^2,
- Temperature T = 200 ºC,
- Atomic diffusivity coefficient D_a = 3e-16 m^2/s,
- Electric driving force $S = EZ^*e/kT$ = 0.04/μm,
- Charge number $|Z^*| = 4$,
- Bulk modulus B = 50 GPa,
- Stress gradient $G = EZ^*e/\Omega$ = 16.5 MPa/μm.

The electrical resistance ρ = 4.079e-8 Ohm·m was derived from the electric driving force S and the current density $J_e = \rho E$. Similarly, the atomic volume Ω = 0.989e-29 m^3 was derived from the value of stress gradient G to obtain the stress results comparable to those in [3].

Because the metal line is embedded in a thick rigid dielectric passivation layer, the line confinement implies the following boundary conditions:

- The atomic flux is blocked at both ends: $J_a = 0$ at $x = 0$ and $x = L$.
- The volume of the conductor is not permitted to change; i.e., the mechanical deformation is zero: $u_x = u_y = 0$.

The model is meshed with the PLANE223 coupled-field elements. In the first set of numerical tests, the electromigration analysis was driven by the electric field alone. Active DOFs were concentration C and electric potential φ. The atomic flux option was used with the migration model. A transient analysis for the time duration of 1e7 seconds was performed to simulate the concentration buildup at the blocking boundaries. Numerical results for the normalized concentration were analogous to those reported by Clement and Lloyd [1] for various conductor lengths L. Results for various values of the electric current density J and the diffusivity coefficient D are presented in Fig. 1 and Fig. 2, respectively.

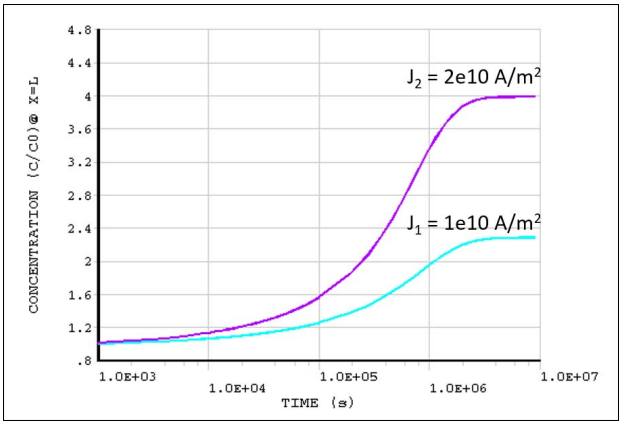

Figure 1. Atomic concentration buildup at $x = L$ for two different current densities J_1 and J_2.

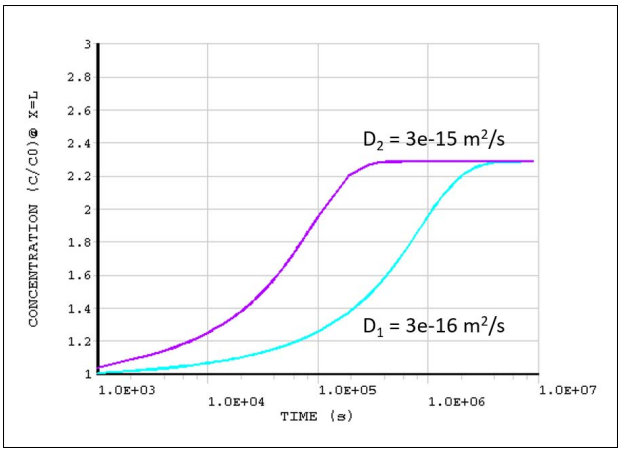

Figure 2. Atomic concentration buildup at $x = L$ for two different diffusion coefficients D_1 and D_2.

Two obvious observations can be made:

- As the only driving force of electromigration, the current density determines the level of concentration at steady-state: the higher the current density, the greater the change in atomic concentration (Fig. 1). For the current density $J_1 = J_e = 1e10$ A/m^2, the normalized concentration varied from 0.3 to 2.3 between the blocking boundaries separated by $L = 50$ μm.
- The diffusivity coefficient controls the time to reach the steady-state: the greater the diffusivity coefficient, the faster the steady-state is reached (Fig. 2). For the atomic diffusivity $D_1 = D_a = 3e\text{-}16$ m^2/s, the time to reach a steady-state concentration takes days. For the vacancy diffusivity coefficient $D_v = 10^7 D_a$ used in [3], the steady-state can be achieved in seconds.

In the next set of numerical tests, displacement DOFs u_x and u_y were activated for the PLANE223 model to include the effect of hydrostatic stress gradient on electromigration.

The mechanical deformation **u** and the total strain **ε** are zero in a confined metal line. Assuming a uniaxial stress state σ_x, it follows from (13) that the hydrostatic stress can be written as:

$$\sigma_H = \frac{1}{3}\sigma_x = \frac{1}{3}E^*\left(-\beta\Delta C\right) = -B\beta\Delta C\,, \tag{28}$$

where $E^* = 3B$ is the Young's modulus. Substituting this expression in (2) and ignoring the thermomigration term, we obtain for the atomic flux in a metal line:

$$\begin{aligned} J_a &= -D\nabla C - \frac{DC\Omega B}{kT}\beta\nabla C - \frac{DCZ^*e}{kT}\nabla\varphi \\ &= -D\left(1 + \frac{DC\Omega B}{kT}\beta\right)\nabla C - \frac{DCZ^*e}{kT}\nabla\varphi, \end{aligned} \tag{29}$$

or

$$J_a = -D_{eff}\nabla C - \frac{D_{eff}CZ^*_{eff}e}{kT}\nabla\varphi \tag{30}$$

where:

$$D_{eff} = D\left(1 + \frac{C\Omega B}{kT}\beta\right) \quad \text{and} \quad Z^*_{eff} = \frac{Z^*e}{1 + \frac{C\Omega B}{kT}\beta} \tag{31}$$

are concentration-dependent effective diffusivity coefficient and charge number. Therefore, electromigration in a 1-D metal line with back stress (28) can be viewed as a mass transport driven by electric field alone (30) and governed by varying diffusivity coefficient D_{eff} and charge number Z^*_{eff} given in (31).

Fig. 3 shows that an electromigration analysis with only diffusion and electric DOFs produces the same concentration buildup as the electromigration analysis with

stress migration if the diffusivity coefficient D and the charge number Z^* are made depended on concentration as in (31).

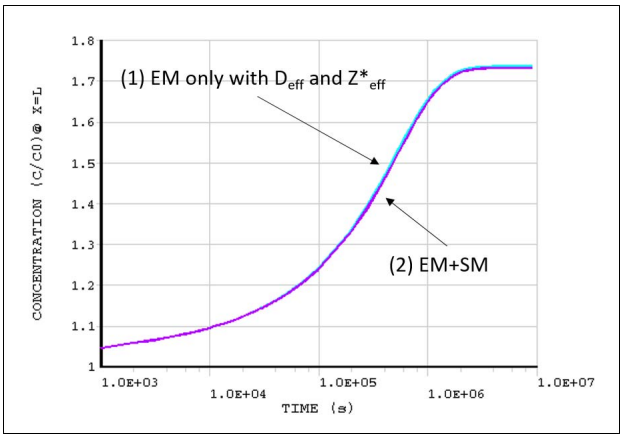

Figure 3. Atomic concentration buildup at $x = L$ driven by (1) the electric force alone with effective diffusivity $Deff$ and effective charge number Z^*_{eff} and by (2) the electric force together with the gradient of hydrostatic stress.

According to (31), including the back stress effect in the model increases the effective diffusivity by the factor of $(1 + C\Omega B\beta/kT)$ and decreases the strength of the electric driving force by the same factor. It was observed earlier that the increase in the effective diffusivity shorten the time to reach the steady-state, while the decrease in the electric driving force diminishes the change in concentration.

This is illustrated in Fig. 4 that compares the buildup of atomic concentration for different β coefficients. For the expansion coefficient β = 5e-2, the steady-state is reached ten times faster than for the model without the back stress effect (β = 0). The change in normalized concentration decreased significantly and varied from 0.86 to 1.14 between the blocking boundaries.

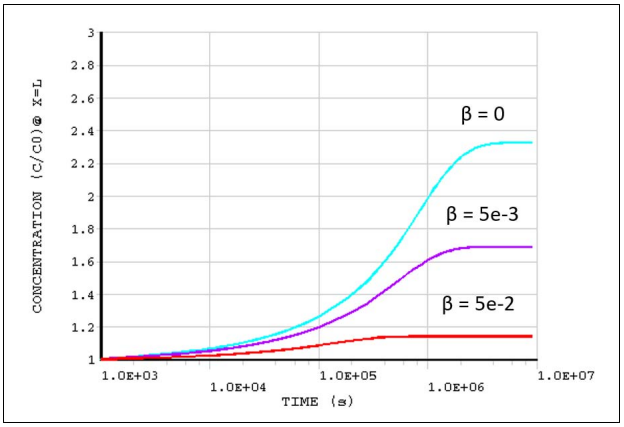

Figure 4. Atomic concentration buildup at $x = L$ for various diffusion expansion coefficients β.

The corresponding hydrostatic stress buidup at $x = 0$ for β = 5e-2 is shown in Fig. 5 together with the analytical solution proposed by Korhonen [3]. The two solutions are not expected to match since Korhonen's stress-concentration relationship is different from (30). According to (30), the maximum stress at steady-state is σ = 350 MPa while Korhonen's estimate that ignores the concentration gradient as a driving force gives $\sigma = GL/2 = 412.5$ MPa.

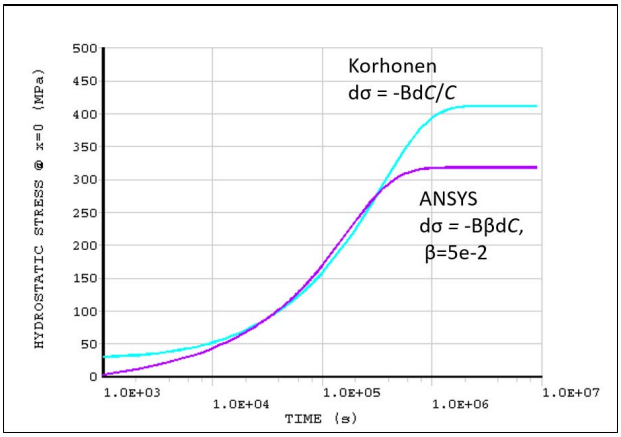

Figure 5. Hydrostatic stress buildup at $x = 0$.

The atomic and vacancy concentration profiles along the length of the metal line are shown in Fig. 6 and 7 at three different moments in time. They show an accumulation of atoms on the anode side of the line and an accumulation of vacancies on the cathode side. The correct direction of the particle transport was enforced by the proper choice of the sign of the charge number Z^* – negative for the atoms and positive for the vacancies.

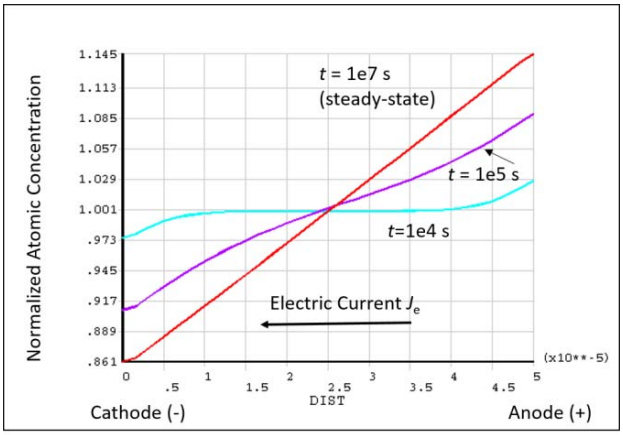

Figure 6. Atomic concentration buidup along the length of the line.

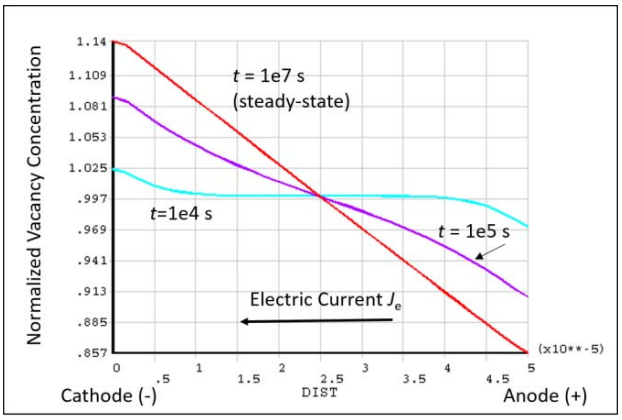

Figure 7. Vacancy concentration buildup along the line.

Both the atomic and vacancy migration models produced the stress profile depicted in Fig. 8. It shows a tensile (positive) stress on the cathode side due to the depletion of atoms and the accumulation of vacancies, and a compressive (negative) stress on the anode side. To ensure the correct sign of the back stress in the simulation, a positive expansion coefficient β was used with the atomic flux model (Table II) and a negative one with the vacancy model (Table III).

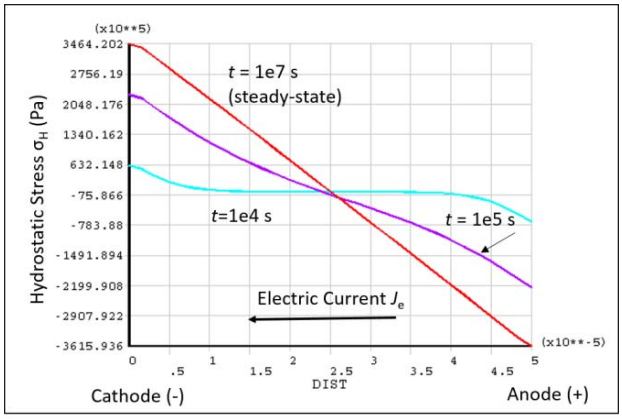

Figure 8. Hydrostatic stress buildup along the length of the line.

VI. Transient Analysis of a Solder Joint

A transient electromigration analysis of a solder joint under a high electric current load is performed to illustrate the combined effect of diffusion, electromigration, stress migration, and thermomigration on the atomic concentration in the solder.

A half symmetry model of a SnAgCu (SAC) solder joint sandwiched between two copper (Cu) conductors is shown in Fig. 9. The diameter of the joint is 760 µm and the standoff height is 450 µm. The width where the solder meets the conductors is 612 µm. These dimensions approximately correspond to the ball grid array (BGA) structure considered in [12]. The conductors are 40 µm thick, 800 µm wide (400 µm in the half symmetry model), and 1000 µm long.

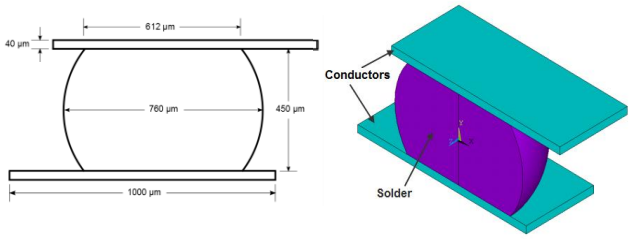

Figure 9. Solder ball model.

The model is meshed with the SOLID226 coupled-field elements. CONTA174 contact elements are defined between the solder joint and the copper conductors. Both SOLID226 and CONTA174 elements have the following DOFs active: concentration (C), electric potential (φ), displacements (u_x, u_y, u_z), and temperature (T). The concentration DOF represents the normalized atomic concentration.

Most of the material parameters for copper and SAC were borrowed from [13] and are listed in Table IV. The pre-exponential diffusivity coeffiecient D_0, activation energy of diffusion Ea and the effective charge number Z^* were selected from [14]. The diffusion expansion coefficients β for diffusion strain calculation were set to 1.e-2 for both materials. The electrical resistivity for copper and SAC was set up to linearly depend on the absolute change in the local normalized concentration C with respect to the eqilibrium concentration C_e: $\rho = \rho_0\left(1+\rho_C\left|C-C_e\right|\right)$, where the dependency and the parameter ρ_C = 2 were arbitrarily chosen.

TABLE IV. Material Properties

Material Property	Cu	SnAgCu
Diffusion		
Diffusivity (pre-exponent) D_0, m^2/s	7.8e-5	4.1e-5
Activation energy E_a, J/mol	210	-
Activation energy E_a, eV	-	0.8
Electric		
Electrical resistivity ρ @135°C, Ohm·m	2.33e-8	17.4e-8
Effective charge number Z^*	-4	-23
Structural		
Young's modulus E, Pa	127.7e9	26.2e9
Poisson's ratio ν	0.31	0.35
Thermal expansion α, 1/K	17.1e-6	23e-6
Diffusion expansion β	1e-2	1e-2
Atomic volume Ω, m^3	1.182e-29	2.71e-29
Thermal		
Thermal conductivity k, W/(m·K)	393	57
Specific heat, J/(kg·K)	385.2	219
Density, kg/m^3	8900	7390
Heat of transport Q, eV	-	0.0094

The electric current of I = 2.85 A (1.425 A for the half symmetry model) is step-applied to the end of one copper lead while the end of the other lead is grounded. This

produces an average current density of 8.9e7 A/m^2 shown in Fig. 10.

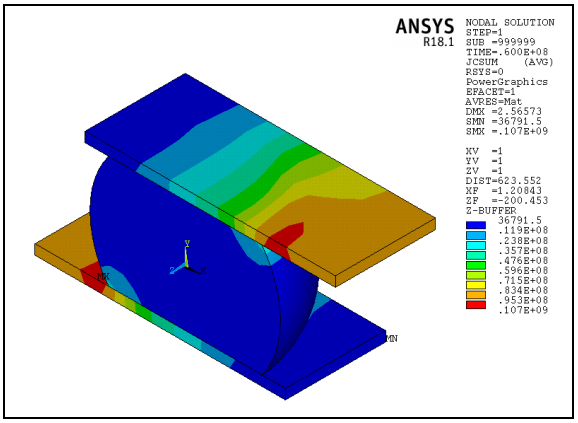

Figure 10. Electric current density (A/m^2).

The structural displacements u_z are constrained on the symmetry surface while the u_y displacements are constrained at the top and bottom surfaces of the model to prevent the structure expansion in the vertical direction.

A convection boundary condition with a film coefficient of 20 W/(m^2 °C) to a bulk temperature of 50°C is specified for all surfaces except the symmetry plane. The temperature offset from absolute zero to zero is set to 273 degrees to evaluate the absolute temperature used in the calculation of the driving forces of electromigration.

A transient analysis with an initial normalized concentration of 1.0 and an initial temperature of 50°C is performed for 60e6 seconds (or approximately 2 years). Diffusion through the copper is very low and electromigration essentially occurs at the interface between the solder and the copper plates. The distribution of the normalized concentration at the end of the simulation (Fig. 11) shows that indeed the atom depletion regions are located at the material interface.

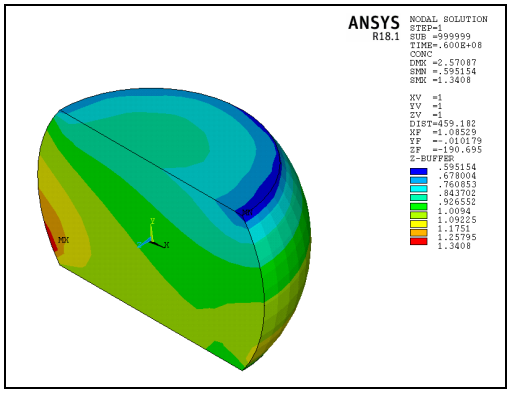

Figure 11. Normalized atomic concentration in the solder.

The analysis shows that a steady-state concentration is reached around 3 months (Fig. 12). A steady-state temperature of 135°C is reached within seconds of the simulation. Because the model is very small and the materials have high thermal conductivities, the temperature is uniform and the temperature gradients do not contribute to atomic diffusion.

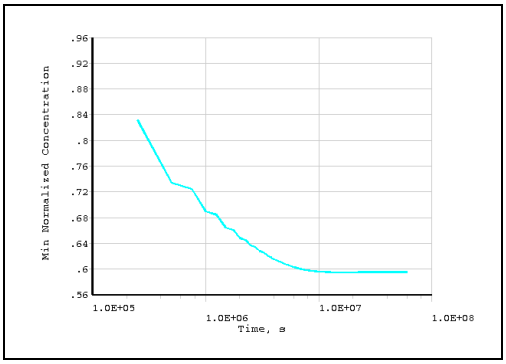

Figure 12. Minimum normalized concentration.

However, the uniform temperature increase does affect atomic migration by contributing to the stress gradients (Fig. 13) due to the displacement constraints on the top and bottom surface of the model and thermal strain incompatibility between the solder and the copper plates.

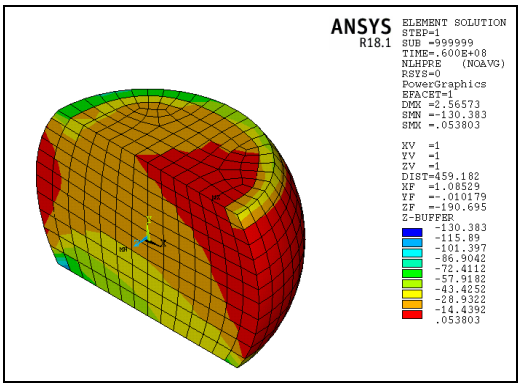

Figure 13. Hydrostatic stress (MPa) in the solder.

The increase in the total electrical resistance R over time is shown in Fig. 14. The increase is due to the dependency of the local resistivity ρ on concentration C specified earlier. The resistivity increase with concentration also affects the atomic transport. Indeed, for a given current density J, higher resistivity results in a higher electric field density $E = \rho J$, thus reinforcing the process of electromigration. This dependency $\rho(C)$, along with the dependency on the hydrostatic stress $\rho(\sigma_H)$, can be used to control the simulation once R reaches a critical level. In other words, these dependencies can serve as electrical failure criteria to determine the TTF of the interconnect.

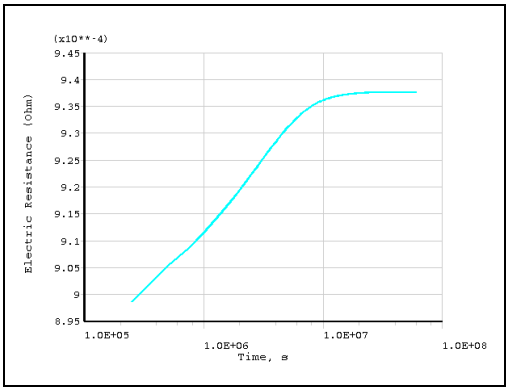

Figure 14. Electrical resistance (Ohm).

CONCLUSIONS

The ANSYS finite element program can now be used to simulate the process of electromigration in metal interconnects. 2-D and 3-D coupled-field elements have been enhanced to support a mass transport of one species – either atoms or vacancies – driven by the electric field and by the gradients of concentration, hydrostatic stress, and temperature. In the developed finite element formulation, concentration is fully (matrix) coupled with the electric potential, mechanical displacements, and temperature by the driving forces of electromigration. Concentration is also fully coupled with the displacements by the diffusion expansion introduced by analogy with thermal expansion to address the deformation produced by the change in concentration.

The electromigration analysis has been extensively tested using 1-D models of metal interconnect lines. Important aspects of the model were discussed using simple 1-D numerical examples previously reported in the literature. A 3-D model of a solder joint is used to demonstrate the electromigration analysis capabilities of predicting the evolution and distribution of concentration, stress, electric current, and temperature.

The ability to make material properties and loads dependent on concentration, hydrostatic stress, temperature, as well as other variables considerably expands the analysis possibilities.

ACKNOWLEDGMENT

The authors would like to thank Dale Ostergaard for encouraging and supporting the work on electromigration and Joann Bryan for reviewing the manuscript.

REFERENCES

[1] J. J. Clement and J. R. Lloyd, "Numerical investigation of the electromagnetic boundary value problem," *J. Appl. Phys*., vol. 71, no. 4, pp. 1729–1731,1992.

[2] R. Kirchheim, "Stress and electromigration in Al-lines of integrated circuits," *Acta metall. Matter*. vol. 40, no, 2, pp. 309-323, 1992.

[3] M.A. Korhonen, P. Borgesen, K.N. Tu, and C.-Y. Li, "Stress evolution due to electromigration in confined metal lines," *J. Appl. Phys*., vol. 73, no. 8, pp. 3790–3799,1993.

[4] Y. Liu, Y. Zhang, and L. Liang, "Prediction of electromigration induced voids and time to failure for solder joint of a wafer level chip scale package," *IEEE Trans. Compon. Package. Technol.*, vol. 33, no.3, pp. 544-552, 2010.

[5] J. Pak, M. Pathak, S. K. Lim, and D. Z. Pan, "Modeling of electromigration in through-silicon-via based 3D IC," *Proc. IEEE Electronic Components and Technology Conference (ECTC 11)*, pp. 1420-1427, 2011.

[6] Y. Hou and C.M. Tan, "Comparison of stress-induced voiding phenomena in copper line-via strctures with different dielectric materials," *Semicond. Sci. Technol*., vol. 24, pp.1-7, 2009.

[7] J. Jing, L. Liang, and G. Meng, "Electromigration simulation for metal lines," *J. Electron. Packaging*, vol.132, pp. 011002-011002-7, 2010.

[8] ANSYS® ANSYS Mechanical Enterprise, Release 18.1, Help System, Theory Reference, Chapter 10. Coupling, ANSYS, Inc.

[9] ANSYS® ANSYS Mechanical Enterprise, Release 18.1, Help System, Element Reference, ANSYS, Inc.

[10] ANSYS® ANSYS Mechanical Enterprise, Release 18.1, Help System, Material Reference, Chapter 5. Multiphysics Material Properties, ANSYS, Inc.

[11] M.E. Sarychev, Yu. V. Zhitnikov, L. Borucki, C.-L. Liu, and T.M. Makhviladze, " General model for mechanical stress evolution during electromigration," *J. Appl. Phys*., vol. 86, no. 6, pp. 3068–3075,1999.

[12] H.Liu, C. Yu, P. Li, and J. Chen, "Current crowding and its effects on electromigration and interfacial reaction in lead-free solder joints," *J. Electron. Packaging*, vol.130, pp.59-63, 2008.

[13] S. Wang and L. Liang, "Solder joint reliability under electromigration and thermal-mechanical load*," Proc. IEEE Electronic Components and Technology Conference (ECTC 07)*, pp. 1074-1083, 2007.

[14] B. Chao, S.-H. Chae, X. Zhang, K.-H. Lu, J. Im, and P.S. Ho "Investigation of diffusion and electromigration parameters for Cu-Sn intermetallic compounds in Pb-free solders using simulated annealing," *Acta Mater*., vol. 55, pp. 2805-2814, 2007.